

PS12: แบบจำลองการทำนายผลอุณหภูมิบริเวณ Pedestal สำหรับ Type III

ELMy H-mode พลาสมา

*วรรณภา บัวงาม¹, สุจินต์ สุวรรณ², ธวัชชัย อ่อนจันทร์², นพพร พูลยรัตน์³ และรพชน พิชา⁴

¹ภาควิชาฟิสิกส์ คณะวิทยาศาสตร์ มหาวิทยาลัยมหิดล E-Mail: pukpuinaruk@hotmail.com

²หน่วยวิจัยพลาสมาและฟิวชัน สถาบันเทคโนโลยีนานาชาติสิรินธร มหาวิทยาลัยธรรมศาสตร์

³ภาควิชาฟิสิกส์ มหาวิทยาลัยธรรมศาสตร์ คลองหลวง ปทุมธานี 12120

⁴สถาบันเทคโนโลยีนิวเคลียร์แห่งชาติ (องค์การมหาชน) จตุจักร กทม. 10900

บทคัดย่อ

การเพิ่มประสิทธิภาพของพลาสมาภายในเครื่องปฏิกรณ์โทคาแมคนั้น วิธีการที่ปฏิบัติคือ การทำให้พลาสมาเข้าไปสู่สภาวะประสิทธิภาพสูงหรือที่เรียกว่า H-mode (High confinement mode) โดยเกิดจากการสร้างความต่างของความดันที่สูงกว่าปรกติในบริเวณเพดสตอล ในการทำนายเงื่อนไขที่บริเวณส่วนบนสุดของเพดสตอลมีความสำคัญต่อการสร้างแบบจำลองในทางทฤษฎีรวมถึงการทดลอง ดังนั้นในงานนี้ คณะทำงานได้พัฒนาแบบจำลองใหม่ขึ้นมาสองแนวทาง เพื่อใช้ทำนายอุณหภูมิที่บริเวณส่วนบนสุดของเพดสตอลในพลาสมาสภาวะประสิทธิภาพสูงแบบมีความไม่เสถียรที่ขอบชนิดที่ 3 แนวทางที่หนึ่งอยู่บนพื้นฐานของทฤษฎี ด้วยการคำนวณพลังงานความร้อนในบริเวณเพดสตอลและการใช้ scaling law ของการกักเก็บพลังงาน (energy confinement) ส่วนแนวทางที่สองอยู่บนพื้นฐานของการทดลองโดยใช้ scaling law กับพารามิเตอร์ที่ควบคุมพลาสมา เช่นกระแสพลาสมา สนามแม่เหล็ก และ กำลังความร้อน ถูกนำมาใช้เพื่อพัฒนาแบบจำลองนี้ แบบจำลองใหม่ทั้งสองนี้จะถูกนำไปทดสอบด้วยวิธีทางสถิติ เช่น ค่าความผิดพลาดรากที่สองของค่าเฉลี่ยกำลังสอง (Root Mean Square) (RMSE) และ ค่าออฟเซต (offset value) กับข้อมูลในฐานข้อมูลเพดสตอลระดับนานาชาติ (Pedestal International Database) ซึ่งพบว่าแบบจำลองแรกที่อยู่บนพื้นฐานของทฤษฎี สามารถทำนายอุณหภูมิของ pedestal โดยมีค่า RMSE อยู่ระหว่าง 30-40% และ scaling law ของ IPB98(y,3) จะให้ค่า RMSE ที่ดีที่สุดโดยมีค่า 30.4% ส่วนแบบจำลองที่สองสามารถทำนายอุณหภูมิของ pedestal โดยมีค่า RMSE เท่ากับ 25.9%

คำสำคัญ: พลาสมา เพดสตอล สภาวะประสิทธิภาพสูงแบบมีความไม่เสถียรที่ขอบชนิดที่ 3 แบบจำลองแบบจำลอง

Pedestal Temperature Model for Type III ELMy H-mode Plasma

W. Buangam^{1*}, S. Suwanna², T. Onjun², N. Poolyarat³, R. Picha⁴, and W. Singhsomroje¹

¹Department of Physics, Mahidol University, Bangkok, Thailand

²Plasma and Fusion Research Unit, Sirindhorn International Institute of Technology,
Thammasat University, Pathumthani, Thailand

³Department of Physics, Thammasat University, Pathumthani, Thailand

⁴Thailand Institute of Nuclear Technology, Bangkok, Thailand

ABSTRACT

It is widely known that the improved performance of *H*-mode plasma results mainly from a formation of an edge transport barrier, called the pedestal, which is a narrow region of strong pressure gradient near the edge of plasma. A predictive capability for the conditions at the top of the pedestal is important, especially for predictive simulations of future experiments. New models for predicting the temperature values at the top of the pedestal for type III ELMy *H*-mode plasma are developed by using three different approaches: one empirical approach and two different theory-based approaches. For an empirical model, a scaling law of pedestal temperature in terms of plasma controlled parameters — including plasma current, magnetic field, heating power, hydrogenic mass, major radius, aspect ratio, and elongation — is deduced from experimental data. For the first theory-based approach, a pedestal model is developed using a calculation of thermal energy in the pedestal region and on accepted scaling laws of energy confinement time. For the second theory-based approach, a pedestal model is developed based on magnetic and flow shear stabilization and ballooning mode pressure gradient limit concept. Predictions from these models are compared with experimental data from the ITPA Pedestal Database version 3.2. Statistical quantities, such as Root-Mean Square Error (RMSE) and offset values, are computed to quantify the predictive capability of the models. It is found that the predictions using an empirical model yield the best agreement among the model developed model with the RMSE of 25.9%. For theory-based models the prediction of the pedestal temperature values are moderately well with the RMSEs between 30% and 42%. The IPB98(y,3) scaling law yields with best agreement among theory-based models with RMSE of 30.4%.

Keywords: Plasma, Pedestal, Type III ELMy *H*-mode, Model

1. INTRODUCTION

Physic of plasma in tokamaks comprises of multiple complicated physical processes on various scales, giving rise to many challenges in modeling tokamak plasma behaviors. In the core region of plasma, where temperature and particle densities are high, physical processes for this region are fairly-well understood. In the outer region of plasma — normally called a pedestal — ,where temperature and particle densities are much lower; the physical processes are governed by atomic physics. The multi-scale processes in plasma require multiple models for different tasks, and these models must be integrated to fully understand plasma behaviors such as temperature and density profiles.

At the top of the pedestal region, pedestal conditions (e.g. temperature, pressure and density) are normally used as boundary conditions in order to predict the core region. These boundary conditions allow one to simulate plasma profiles from the pedestal point inward to the center^{1, 6}. Pedestal temperature models have been shown to provide satisfactory predictions of boundary conditions in *H*-mode plasma discharges, especially those related to Edge Localized Modes (ELMs)^{10, 11}. ELMs are commonly found in magnetically confined plasma experiments, where it is observed that the plasma periodically peels itself off like an avalanche, often called ELM crashes, leading to rapid (of the millisecond order) losses of plasma energy and particles (roughly 5-10%)^{4, 9, 12, 15}. ELMs are believed to be caused by MHD instability occurred near the edge of *H*-mode plasma. Repetitive ELMs generally degrade the global particle and energy confinement time and deposit high loads on the divertor plates causing them to erode quickly. However, ELMs can also be beneficial in removing plasma impurities at the edge of plasma¹⁵.

In general, ELMs can be detected from measuring plasma energy or H_{α} or D_{α} signals^{9, 15}, and are classified into three types (denoted by type I, type II and type III) according to the dependence of repetition frequency on heating power; the occurrence of magnetic precursors; and the MHD instability with respect to the ideal ballooning criterion. See Reference no. 12,14,15 for more details.

It should be remarked here that type III ELMs are sometimes called *small* ELMs, where the frequency decreases as heating power increases. In type III ELMs, the plasma edge pressure is significantly below the ideal ballooning limit, and the magnetic precursor oscillation is coherent with frequency around 50–70 kHz¹⁵. Compared with type I, a type III ELM corresponds to lower pressure gradient prior to the crash, but to a significantly higher frequency. Generally, a type III crash produces less energy and particle losses than a type I crash⁹.

Previously, pedestal temperature models have been developed for type I ELMy *H*-mode plasma. In this work, the pedestal temperature model is developed for a type III ELMy *H*-mode plasma. The pedestal temperature models based on energy distribution using accepted *H*-mode scaling laws of energy confinement time as well as an empirical temperature model are developed to predict pedestal temperature values from five tokamaks. The predicted results are compared with experimental results from the ITPA Pedestal Database (Version 3.2)². Then¹, statistical analyses such as root-mean-square errors (RMSE) and offset values are calculated to quantify the agreement.

This article is organized into four parts. A pedestal temperature model based on energy distribution with H -mode scaling laws and a pedestal temperature model base on magnetic and flow shear stabilization with width scaling are described in Section 2. The results and discussions from our statistical analysis are included in Section 3 as well as an empirical pedestal temperature model. Finally, conclusions are summarized in Section 4.

2. MODELING

2.1 PEDESTAL TEMPERATURE MODEL BASED ON ENERGY DISTRIBUTION

The energy loss mechanism from the pedestal comes mainly from the thermal conduction down the steep edge gradient characterizing the pedestal region. The thermal energy at the pedestal can be taken as

$$W_{ped} = c_1 n_{ped} k T_{ped} V \quad (1)$$

where n_{ped} is the pedestal density; k is Boltzmann's constant; T_{ped} is the pedestal temperature; and V is the plasma volume, which can be estimated by

$$V = 2\pi^2 R a^2 \kappa \left(1 - \frac{\delta a}{4R} - \frac{\delta^2}{4} \right) \quad (2)$$

where \mathbf{K} and $\mathbf{\delta}$ are, respectively, the elongation and triangularity at the separatrix, respectively; R and a are major radius and minor radius, respectively, of a tokamak. The constant c_1 is often taken to be 2 or 3.

Moreover, W_{ped} can also be computed from the total thermal energy W_{th} in the system; namely,

$$W_{ped} = c_2 W_{th} \quad (3)$$

where c_2 is a fraction of total thermal energy at the pedestal and is often estimated by taking as $c_2 = 0.35$. Here we leave the constants c_1 and c_2 undetermined.

In addition, the release of thermal energy depends directly on the energy confinement time τ_E and the power supplied to the plasma. As such, it follows that

$$\tau_E = c_3 \frac{W_{th}}{P_{aux}}$$

(4)

where P_{aux} is an auxiliary heating power, which generally comes from neutral beam injection (NBI) or radio frequency (RF) heating. Combining Eq. (1)–(4), the resulting pedestal temperature is

$$T_{ped} = C_E \frac{P_{aux} \tau_E}{n_{ped} kV}$$

(5)

where C_E is now an overall constant, which will be determined as to minimize the root-mean-square errors (RMSE) of predicted results when they are compared with experimental data. In Eq. (5), all relevant quantities, except τ_E , are known from each tokamak; and they describe either experimental scheme or the geometry of plasma in the tokamak.

2.2 SCALING LAWS FOR *H*-MODE PLASMA

The quantity τ_E is deduced in various ways from many experiments. There already exist several scaling laws that express τ_E in terms of plasma engineering parameters^{4, 12, 14} as published by the ITER Physics Basis (IPB) group⁷. Here we employ with four well-known scaling laws whose expressions of the thermal energy confinement time τ_E of ELMy *H*-mode plasma are included below.

In the following expressions, I denotes current in MA; B toroidal field in T; P power in MW; n density in ($\times 10^{19} m^{-3}$); R major radius in m ; M effective mass in amu . An inverse aspect ratio, $\varepsilon = a/R$, and elongation \mathcal{K} are dimensionless.

$$\tau_{ITERH-93P} = 0.036 I^{1.06} B^{0.32} P^{-0.67} n^{0.17} R^{1.79} \varepsilon^{-0.11} \mathcal{K}^{0.66} M^{0.41}$$

$$\tau_{ITERH-ESP97(y)} = 0.029 I^{0.90} B^{0.20} P^{-0.66} n^{0.40} R^{2.03} \varepsilon^{0.19} \mathcal{K}^{0.92} M^{0.2}$$

$$\tau_{IPB98(y,3)} = 0.0564 I^{0.88} B^{0.07} P^{-0.69} n^{0.40} R^{2.15} \varepsilon^{0.64} \mathcal{K}^{0.78} M^{0.2}$$

$$\tau_{IPB98(y,4)} = 0.0587 I^{0.85} B^{0.29} P^{-0.70} n^{0.39} R^{2.08} \varepsilon^{0.69} \mathcal{K}^{0.76} M^{0.17}$$

More details and excellent overviews of these scaling laws can be found in^{3, 5, 7, 8, 13}.

In addition to the pedestal temperature model based on energy distribution and on *H*-mode scaling laws for τ_E , we also investigate empirical pedestal temperature model by fitting pedestal temperature values from five tokamaks: AUG, DIII-D, JET, JT60U and MAST. The details of this empirical model will be provided in the next section.

2.3. SCALING OF PEDESTAL WIDTH

The temperature at the top of pedestal can be written in terms of the maximum normalized pressure gradient that is the critical pressure gradient, α_c ,

$$T_{\text{ped}} = \frac{\Delta}{2kn_{\text{ped}}} \frac{\alpha_c B_T^2}{2\mu_0 R q^2} \quad (6)$$

where Δ is the pedestal width, μ_0 is the permeability of free

space, $\alpha_c = 0.8s \frac{1 + \kappa_{95}^2 (1 + 5\delta_{95}^2)}{2}$ and the safety factor

$$q(x) = \frac{q_{95}}{\left[\left(1 + \left(\frac{0.95}{1.4} \right)^2 \right)^2 + 0.267 |\ln(1 - 0.95)| \right] \left[\left(1 + \left(\frac{x}{1.4} \right)^2 \right)^2 + 0.267 |\ln(1 - x)| \right]}$$

In this paper, five theory models for the pedestal width (see¹⁶ for more details) are applied in determining the pedestal temperature, then the result are compared with experimental data.

A. Width scaling 1 – based on magnetic and flow shear stabilization

The scaling of the pedestal width is

$$\Delta = C_1 \rho s^2 = C_1 \left(4.57 \times 10^{-3} \frac{\sqrt{A_H T_{\text{ped}}}}{B_T} \right) s^2, \quad (7)$$

where ρ is the ion gyro radius, A_H is the average hydrogenic mass. By using this scaling for the pedestal width in Eq. (6), the temperature at the top of pedestal can be obtained from

$$T_{\text{ped}} = C_1^2 \left(\left(\frac{4.57 \times 10^{-3}}{4\mu_0 (1.6022 \times 10^{-6})} \right)^2 \left(\frac{B_T^2}{q^4} \right) \left(\frac{A_H}{R^2} \right) \left(\frac{\alpha_c}{n_{\text{ped}}} \right)^2 s^4 \right),$$

(8)

where C_1 is the constant of proportionality in Eq. (7).

B. Width scaling 2 – based on flow shear stabilization

The scaling of the pedestal width is

$$\Delta = C_2 \sqrt{\rho R q}$$

(9)

By using this scaling for the pedestal width in Eq. (6), the temperature at the top of pedestal can be determined from

$$T_{\text{ped}} = C_2^{4/3} \left(\left(\frac{(4.57 \times 10^{-3})^{1/2}}{4\mu_0 (1.6022 \times 10^{-16})} \right)^{4/3} \left(\frac{B_T}{q} \right)^2 \left(\frac{\sqrt{A_H}}{R} \right)^{2/3} \left(\frac{\alpha_c}{n_{\text{ped}}} \right)^{4/3} \right) \quad (10)$$

C. Width scaling 3 – based on normalized poloidal pressure

The scaling of pedestal width is

$$\Delta = C_3 \sqrt{\beta_\theta} R = C_3 \sqrt{\frac{4\mu_0 n_{\text{ped}} k T_{\text{ped}}}{\langle B_\theta \rangle^2}} R, \quad (11)$$

where β_θ is the normalized poloidal pressure and $\langle B_\theta \rangle$ is the average poloidal field around the flux surface. By using this scaling for the pedestal width in Eq. (6), the temperature at the top of pedestal can be obtained from

$$T_{\text{ped}} = C_3^2 \left(\left(\frac{1}{4\mu_0 (1.6022 \times 10^{-16})} \right) \left(\frac{B_T}{q} \right)^2 \left(\frac{R}{a} \right)^2 \left(\frac{\alpha_c^2}{n_{\text{ped}}} \right) \left(\frac{\pi q_{95} (1 + \kappa_{95})}{5g_s} \right)^2 \right) \quad (12)$$

where q_{95} , the safety factor at the 95% flux surface, with geometrical effects included, is defined by

$$q_{95} \equiv \frac{5a^2 B_T}{\mu_0 I_p R} g_s(\kappa_{95}, \delta_{95}, \varepsilon), \text{ and the geometrical factor, } g_s, \text{ is taken to be}$$

$$g_s(\kappa_{95}, \delta_{95}, \varepsilon) = \frac{\left[1 + \kappa_{95}^2 (1 + 2\delta_{95}^3 - 1.2\delta_{95}^3) \right] (1.17 - 0.65\varepsilon)}{2(1 - \varepsilon^2)^2} \text{ which shaping effects, } \kappa_{95} \text{ is}$$

elongation at the 95% flux surface and is taken to be 0.914 times the value of the elongation at the separatrix, triangularity δ_{95} (assumed to be approximately 0.85 times the value of triangularity at the separatrix).

D. Width scaling 4 – based on diamagnetic stabilization

The scaling of pedestal width is

$$\Delta = C_4 \rho^{2/3} R^{1/3}. \quad (13)$$

By using this scaling for the pedestal width in Eq. (6), the temperature at the top of pedestal can be obtained from

$$T_{\text{ped}} = C_4^{3/2} \left(\left(\frac{(4.57 \times 10^{-3})^{2/3}}{4\mu_0 (1.6022 \times 10^{-6})} \right)^{3/2} \left(\frac{B_T^2}{q^3} \right) \left(\frac{\sqrt{A_H}}{R} \right) \left(\frac{\alpha_c}{n_{\text{ped}}} \right)^{3/2} \right) \quad (14)$$

E. Width scaling 5 – base on ion orbit loss

The scaling of pedestal width is

$$\Delta = C_5 \sqrt{\varepsilon} \rho_\theta \approx C_5 \varepsilon^{-1/2} q \rho / \kappa_{95} \quad (15)$$

where ρ_θ is the ion poloidal gyro radius and s_{orbit} is a term due to squeezing of the banana orbits by the radial electric field. By using this scaling for the pedestal width in Eq. (6), the temperature at the top of pedestal can be obtained from

$$T_{\text{ped}} = C_5^2 \left(\left(\frac{(4.57 \times 10^{-3})}{4\mu_0 (1.6022 \times 10^{-16})} \right)^2 \left(\frac{B_T}{q} \right)^2 \left(\frac{A_H}{\kappa_{95}^2 a R} \right) \left(\frac{\alpha_c}{n_{\text{ped}}} \right)^2 \right) \quad (16)$$

3. RESULTS AND DISCUSSION

3.1 PREDICTIONS FROM EMPIRICAL PEDESTAL TEMPERATURE MODEL

As these scaling laws in the previous section do not predict pedestal temperature values that agree satisfactorily with experimental data, it is useful and perhaps necessary to explore alternatives for a pedestal temperature model. In the following, we investigate an empirical pedestal temperature model by fitting experimental pedestal temperature from the mentioned five tokamaks in terms of plasma engineering parameters. Like before, we shall assume that the energy confinement time depends on plasma parameter of the form:

$$\tau_E \propto B^{\alpha_B} I^{\alpha_I} M^{\alpha_M} P^{\alpha_P} R^{\alpha_R} \varepsilon^{\alpha_\varepsilon} \kappa^{\alpha_\kappa}$$

Therefore,

$$T_{\text{ped}} = \frac{C_E}{k} n^{\alpha_n} V^{\alpha_V} B^{\alpha_B} I^{\alpha_I} M^{\alpha_M} P^{\alpha_P} R^{\alpha_R} \varepsilon^{\alpha_\varepsilon} \kappa^{\alpha_\kappa}$$

The values of C_E and all alphas are determined from best (multiple) linear regression using the Origin Pro software. It is found the lowest RMSE% is below 25.94%, when the values of exponents are given in Table 1.

Table 1: Optimal values of parameters from empirical scaling of T_{ped} in Eq. (17) are listed as well as the RMSE and offset values.

| | | | |
|---------------|-------------|---------------|--------------|
| C_E | 2.49 | α_M | 0.40 |
| α_n | -0.84 | α_P | 0.44 |
| α_V | -1.13 | α_R | 2.25 |
| α_B | 0.01 | α_E | 0.71 |
| α_I | 0.97 | α_K | 2.62 |
| RMSE % | 25.9 | Offset | 0.004 |

The statistical analysis of ratios of predicted temperature values from Eq. (17) to experimental ones is shown in Figure 1.

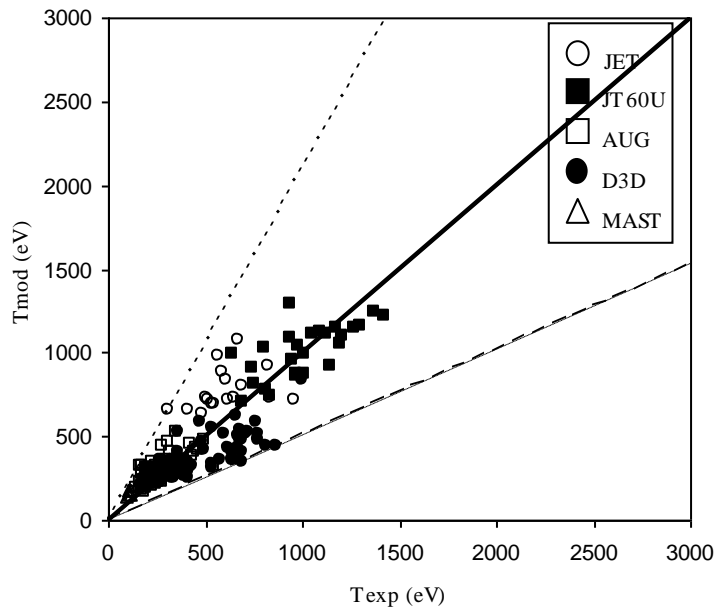


Figure 1. Predicted pedestal temperature values in the empirical model Eq. (17) are plotted as a function experimental pedestal temperature values.

In Figure 1, it is shown that the predicted temperature values agree well with data from DIII-D tokamak (similar to Figures 1–4), but poorly with those from JET tokamak. For this model, the lower and upper bounds are given as

$$0.51T_{\text{exp}} \leq T_{\text{mod}} \leq 2.10T_{\text{exp}} \quad (18)$$

It should be remarked that the empirical model Eq. (17) yields the scaling $V^{1.13}$ for volume, instead of V^1 in Eq. (5). This is a possible reason for an improved RMSE% from over 30% to below 26%. At minimum, this model clearly improves the predictions of JT60U pedestal temperature values.

3.2 PREDICTIONS FROM PEDESTAL TEMPERATURE MODEL BASED ON ENERGY DISTRIBUTION

The predicted results of pedestal temperature values from the model based on energy distribution coupled with the aforementioned scaling laws are included in Table 2.

Table 2: Optimal values of C_E and their corresponding RMSE% and offset values from each scaling law are listed.

| Scaling | C_E | RMSE % | Offset |
|--------------|-------|--------|--------|
| ITERH-93P | 0.069 | 41.1 | -0.098 |
| ITERH-EPS97y | 0.073 | 34.1 | -0.060 |
| IPB98(y,3) | 0.073 | 30.4 | -0.061 |
| IPB98(y,4) | 0.071 | 33.0 | -0.071 |

From Table 2, it is evident that the IPB98(y,3) scaling law for energy confinement time gives best agreement overall for all five tokamaks, but it only implies moderate agreement with experiments, yielding RMSE of 30.4%.

It is found that, as expected, the model does not necessarily yield the same agreement from one tokamak to another. The statistical analysis of ratios of experimental temperature to predicted temperature for these scaling laws on individual tokamaks is shown in Figures 2–5. In these figures, solid circles denote data points from DIII-D tokamak, open circles from JET, solid squares from JT60U, open squares from AUG and open triangles from MAST. In addition, the lower and upper dashed lines give, respectively, lower and upper bounds of predicted pedestal temperature, denoted

by T_{mod} by a linear function of experimental temperature T_{exp} . Clearly, the closer the lower and upper bounds are together, the more accurate the model predicts the pedestal temperature values. The middle solid line is the ultimate goal which gives $T_{mod} = T_{exp}$.

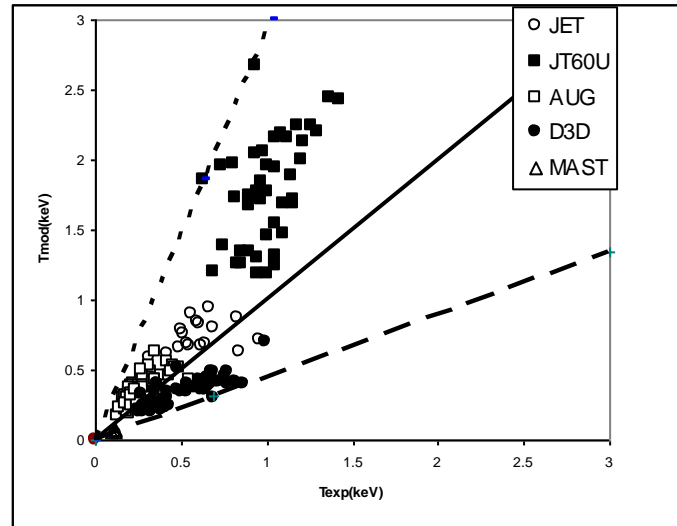


Figure 2. Using ITERH-93P scaling law, predicted pedestal temperature values are plotted versus experimental pedestal temperature values.

In Figure 2, it is found that the predicted temperature values agree well with data from DIII-D, but poorly with those from JT60U. For the ITERH-93P scaling law, T_{mod} can be given in terms of lower and upper bounds as

$$0.45T_{exp} \leq T_{mod} \leq 2.92T_{exp} \quad (17)$$

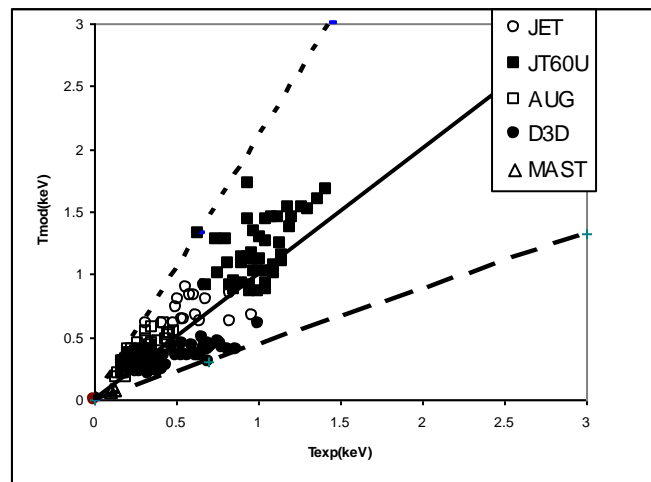


Figure 3. Using ITERH-EPS97y scaling law, predicted pedestal temperature values are plotted as a function experimental pedestal temperature values.

In Figure 3, it is found that the predicted pedestal temperature values agree well with data from DIII-D, but poorly with those from JT60U. However, unlike in Figure 2, here the lower and upper bounds are closer together, and the JT60U predictions clearly lie closer to the solid line. For ITERH-EPS97y, the predicted temperature values can be given in terms of lower and upper bounds as

$$0.44T_{\text{exp}} \leq T_{\text{mod}} \leq 2.08T_{\text{exp}} \quad (18)$$

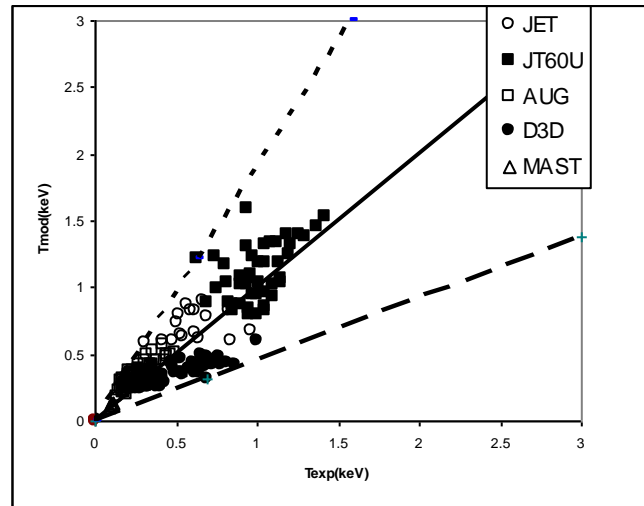


Figure 4. Using IPB98(y,3) scaling law, predicted pedestal temperature values are plotted as a function of experimental pedestal temperature values.

In Figure 4, it is found the IPB98(y,3) scaling law yields qualitatively the same trends as the ITERH-EPS97y scaling law does. IPB98(y,3) yields lower RMSE% than ITERH-EPS97y because its upper bound is lower than that corresponding to ITERH-EPS97y. Specifically, the IPB98(y,3) lower and upper bounds are given by

$$0.46T_{\text{exp}} \leq T_{\text{mod}} \leq 1.91T_{\text{exp}} \quad (19)$$

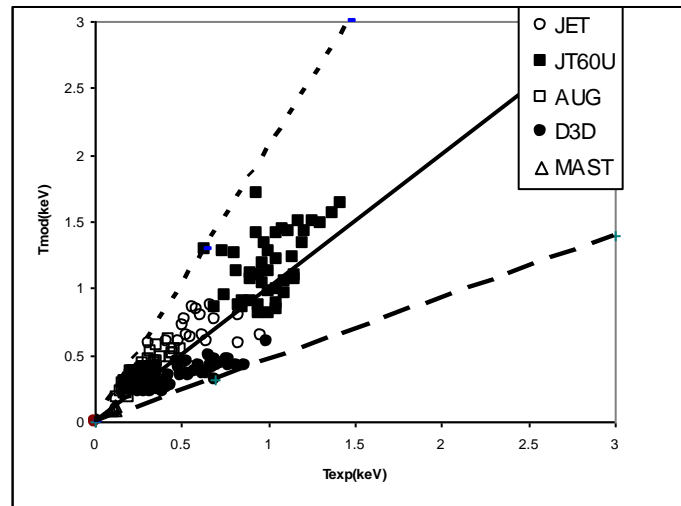


Figure 5. Using IPB98(y,4) scaling law, predicted pedestal temperature values are plotted versus experimental pedestal temperature values.

In Figure 5, it is found that the predicted temperature values agree well with data from DIII-D, but poorly with those from JT60U. The predictions from the IPB98(y,4) scaling law are very similar to the previous two scaling law, with the same lower bound and slight different upper bound. Here, for IPB98(y,4), the lower and upper bounds are given by

$$0.46T_{\text{exp}} \leq T_{\text{mod}} \leq 2.04T_{\text{exp}} \quad (20)$$

It should be remarked from Figures 2–5 that the model based on energy distribution and on *H*-mode scaling laws tends to over predict pedestal temperature values in AUG, JET and JT60U, but to under predict those from DIII-D. Overall, predictions for DIII-D are more coherent and yield best agreement, while predictions for JT60U are most dispersed and lie significantly above the ideal line $T_{\text{mod}} = T_{\text{exp}}$.

3.3 PREDICTIONS FROM PEDESTAL TEMPERATURE MODEL BASED ON MAGNETIC AND FLOW SHEAR STABILIZATION

The predicted results of pedestal temperature values from the models based on magnetic and flow shear stabilization are included in Table 3.

Table 3: Coefficients and RMSE of the models from each scaling width for type III ELMy H-mode discharges.

| Model | Width scaling | C_w | RMSE(%) |
|-------|---|-------|---------|
| 1a | $\Delta \propto \rho s^2$ | 0.90 | 48.1 |
| 2a | $\Delta \propto \sqrt{\rho R q}$ | 0.15 | 48.0 |
| 3a | $\Delta \propto \sqrt{\beta_\theta} R$ | 0.02 | 53.7 |
| 4a | $\Delta \propto \rho^{\frac{2}{3}} R^{\frac{1}{3}}$ | | |
| 5a | $\Delta \propto \sqrt{\epsilon \rho_\theta}$ | 1.84 | 50.2 |

From Table 3, it is evident that the RMSE ranges from 48.0% to 53.7%. Model 2a yields the lowest RMSE and Model 3a yields the highest RMSE.

The statistical analysis of the ratios of experimental temperature to predicted temperature for each scaling width on individual tokamaks is shown in Figures 6-9.

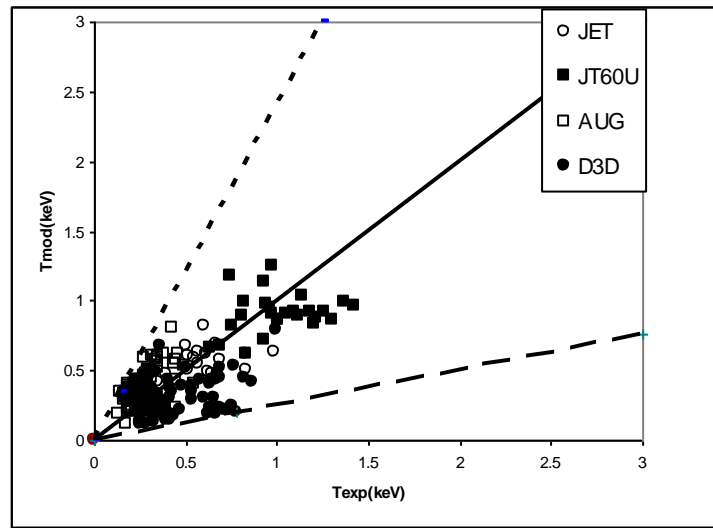


Figure 6. Using Model 1a ($\Delta \propto \rho s^2$), predicted pedestal temperatures are plotted versus experimental pedestal temperatures.

In Figure 6, it is found that the predicted temperature values agree well with all data. For the Model 1a, T_{mod} can be given in terms of lower and upper bounds as

$$0.25T_{exp} \leq T_{mod} \leq 2.41T_{exp} \quad (21)$$

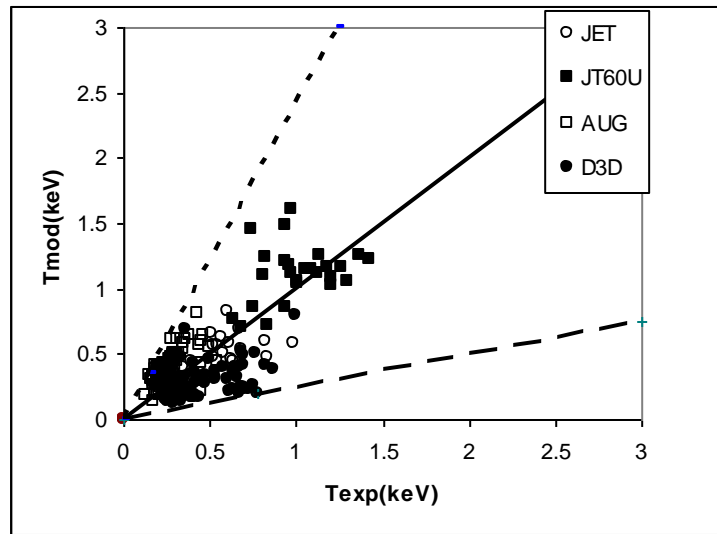


Figure 7. Using Model 2a ($\Delta \propto \sqrt{\rho R q}$), predicted pedestal temperatures are plotted as a function of experimental pedestal temperatures.

In Figure 7, it is found that the predicted pedestal temperature values agree well with data from DIII-D, but poorly with those from JT60U. For model 2a, the predicted temperature values can be given in terms of lower and upper bounds as

$$0.25T_{\text{exp}} \leq T_{\text{mod}} \leq 2.41T_{\text{exp}} \quad (22)$$

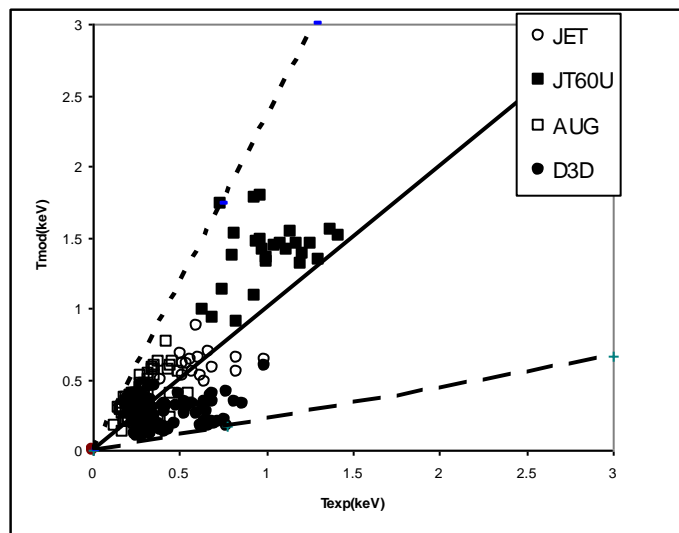


Figure 8. Using Model 3a ($\Delta \propto \sqrt{\beta_0 R}$), predicted pedestal temperatures are plotted as a function of experimental pedestal temperatures.

In Figure 8, it is found that the predicted pedestal temperatures are the same as those in Model 2a but fit very poorly with JT60U data. For Model 2a, the predicted temperature values can be given in terms of lower and upper bounds as

$$0.22T_{\text{exp}} \leq T_{\text{mod}} \leq 2.35T_{\text{exp}} \quad (23)$$

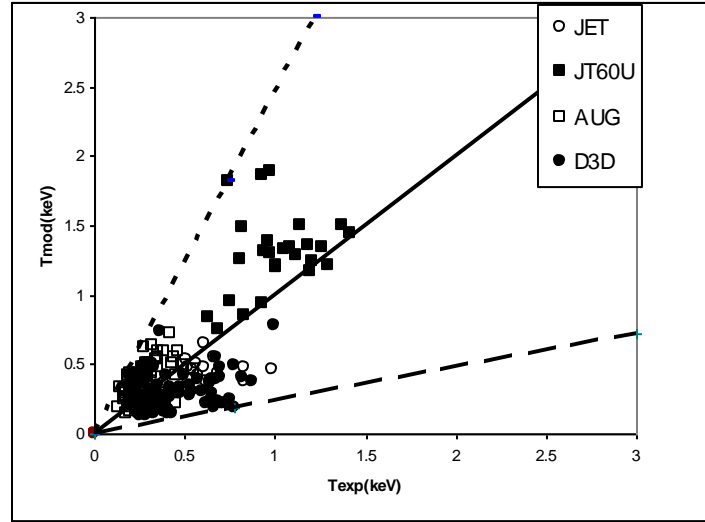


Figure 9. Using Model 5a ($\Delta \propto \sqrt{\varepsilon\rho_0}$) predicted pedestal temperatures are plotted as a function of experimental pedestal temperatures.

In Figure 9, it is found that the predicted pedestal temperature values are the same in Model 2a but very poor agreement with JT60U data. For Model 5a, the predicted temperature values can be given in terms of lower and upper bounds as

$$0.24T_{\text{exp}} \leq T_{\text{mod}} \leq 2.45T_{\text{exp}} \quad (24)$$

4. CONCLUSION

A pedestal temperature model based on thermal energy distribution coupled with well-known scaling laws for energy confinement time τ_E computes pedestal temperature values for type III ELMy *H*-mode plasma which agree moderately well with experimental data, yielding RMS between 30% and 42%. This model tends to over predict results from AUG, JET and JT60U, but under predict those from DIII-D. Using a pedestal temperature model based on magnetic and flow shear stabilization with width scaling, the predicted pedestal temperature value are between 48% and 53% of RMSE.

An alternative empirical pedestal temperature model is investigated. By fitting many experimental results from five tokamaks, it is found that the empirical temperature model predicts the pedestal temperature values with RMSE of 25.9%.

5. ACKNOWLEDGEMENTS

W.B. would like to thank the Development and Promotion of Science and Technology (DPST) scholarship and Mahidol University for their supports. S.S. would like to thank Thammasat University for research fund under contract number TU 35/2551.

6. REFERENCES

1. G. Bateman et al, Phys. Plasmas, **5** (1998), 1793.
2. D. Boucher et al, Nucl. Fusion, **40** (2000), 1955.
3. J. G. Cordey et al, Nucl. Fusion, **39** (1999), 301–307.
4. J. Freidberg, Plasma Physics and Fusion Energy, Cambridge Univ. Press, Cambridge, 2007.
5. R. J. Goldston, Plasma Phys. Control. Fusion, **26** no. 1A (1984), 87.
6. D. Hannum et al, Phys. Plasmas, **8** (2001), 964.
7. ITER Physics Basis, Nucl. Fusion, **47** (2007), S18.
8. D. McDonald et al, Nucl. Fusion, **47** (2007), 147.
9. T. Onjun, Ph. D. Thesis, Lehigh University, 2004.
10. T. Onjun et al, Phys. Plasmas, **8** (2001), 975.
11. T. Onjun et al, Phys. Plasmas **9** (2002), 5018.
12. W. M. Stacey, Fusion Plasma Physics, WILEY-VCH Verlag GmbH & Co. KgaA, Weinheim, 2005.
13. N. A. Uckan, Workshop on Physics Issues for FIRE, May 1–3, 2000, Princeton, NJ.
14. J. Wesson, Tokamaks, 3rd Edition, Clarendon Press, Oxford, 2004.
15. H. Zohm, Plasma. Phys. Control. Fusion, **38** (1996), 105–128.
16. T. Onjun et al, Phys. Plasmas **9** (2002), 5019.